

Functional Connectivity in Single and Multislice Echoplanar Imaging Using Resting-State Fluctuations²

M. J. Lowe,¹ B. J. Mock, and J. A. Sorenson

Department of Medical Physics, University of Wisconsin, Madison, Wisconsin

Received May 16, 1997

A previous report of correlations in low-frequency resting-state fluctuations between right and left hemisphere motor cortices in rapidly sampled single-slice echoplanar data is confirmed using a whole-body echoplanar MRI scanner at 1.5 T. These correlations are extended to lower sampling rate multislice echoplanar acquisitions and other right/left hemisphere-symmetric functional cortices. The specificity of the correlations in the lower sampling-rate acquisitions is lower due to cardiac and respiratory-cycle effects which are aliased into the pass-band of the low-pass filter. Data are combined for three normal right-handed male subjects. Correlations to left hemisphere motor cortex, visual cortex, and amygdala are measured in long resting-state scans. © 1998 Academic Press

Key Words: functional magnetic resonance imaging; functional connectivity; physiologic noise; motor cortex; visual cortex; amygdala.

INTRODUCTION

The human brain operates as a sophisticated network of approximately 10^{12} neurons. Cytoarchitectonic studies of the human brain have identified approximately 50 functionally distinct cortical regions. An extensive network of fibers connects the different cortical regions. Until recently, postulates about the functional association of these different cortical regions has relied on animal models and inference from the density of fiber connections.

Disruptions in corticocortical connectivity in the human brain are cited as sources of cognitive, neurologic, and behavioral dysfunction. Interhemispheric connectivity abnormalities such as agenesis of the corpus

callosum lead to “disconnection” syndromes, which result in impairment of complex motor, visual, auditory, and even higher cognitive function such as semantic processing (Siddis *et al.*, 1981; Davidson *et al.*, 1990; Davidson and Saron, 1992).

Measures of corticocortical connectivity of the human brain play an important role in understanding both ordinary and diseased brain function.

Coherence in the frequency spectrum of electroencephalography (EEG) studies on subjects in a resting state has been used as a measure of functional coupling across distinct regions of the human brain (Thatcher *et al.*, 1986; Tucker *et al.*, 1986). In particular, studies have shown that the coherence of EEG between the right and the left hemispheres is diminished in acallosal and callosotomized subjects when compared to neurologically normal populations (Neilson *et al.*, 1993; Koeda *et al.*, 1995). This measure of synchrony in EEG data is seen to correlate positively with many factors associated with directness of neuronal connectivity. For example, EEG coherence has been shown to increase with the degree of callosal maturation (Farber and Knyazeva, 1991). Also, Scher *et al.* (1994) have shown that the coherence of various inter- and intrahemispheric EEG spectra is greater in preterm infants than in full-term infants, when measured at the same post-conceptual age. The authors interpret this as an indication of increased neuronal connectivity due to extrauterine experience. The lack of spatial resolution in standard scalp-recording EEG studies prohibits studies of coherence between specific cortical structures.

The concept of functional connectivity has been introduced into the functional neuroimaging literature as a descriptive measure of spatiotemporal correlations between spatially distinct regions of cerebral cortex (Friston *et al.*, 1993; Strother *et al.*, 1995). Although, thus defined, functional connectivity does not necessarily reflect a causal relationship between cortical regions, it can provide a useful characterization of cortical interactions (Friston *et al.*, 1996b).

Positron emission tomography (PET) studies regarding functional connectivity have typically relied on a

¹ Division of Imaging Science, Department of Radiology, Indiana University School of Medicine, CL120, 541 Clinical Drive, Indianapolis, Indiana 46202-5111.

² Portions of this work were presented at the 2nd International Conference on Functional Mapping of the Human Brain, Boston, MA, June 17–21, 1996.

posteriori observations of associated activated cortical regions in task-driven functional neuroimaging studies. Two exceptions to this are Horwitz (1991) and Paus *et al.* (1997). Horwitz studied correlations in resting-state PET data as a measure of functional association in human cortex. He found a reduction in resting-state correlations between frontal lobe and parietal lobe between age-matched groups of controls and those with dementia of the Alzheimer's type. Paus *et al.* combined PET and transcranial magnetic stimulation (TMS) in a novel manner in order to assess neuronal connectivity through direct stimulation of the frontal eye fields and subsequent observation of increased regional cerebral blood flow throughout the brain. The authors find that in addition to increased blood flow in the stimulated area, there is significant increase in blood flow to the parieto-occipital cortex of the ipsilateral hemisphere—a region known to have anatomic connection to the frontal eye fields in the monkey. The authors state that their method is a more direct test of neuronal connectivity since correlational analyses from task-driven studies may not show actual neuronal connectivity, but rather concurrent neuronal activation resulting from the task itself.

The sensitivity and temporal resolution of functional magnetic resonance imaging (fMRI) make it an ideal modality for assessing functional connectivity. The source of the fluctuations seen in BOLD-weighted fMRI acquisitions is oxygenation fluctuations in cerebral tissue perfused with arteries and branching arterioles, capillaries, and venules. Observations of physiologic-based sources of fluctuation in blood oxygenation level dependent (BOLD)-weighted MR time series data have been made almost since the inception of the technique (Jezzard *et al.*, 1992; Weisskoff *et al.*, 1993). The fluctuations from cardiac and respiratory cycles are clearly evident in BOLD-weighted MR time series measurements. Figure 1 shows the Fourier power spectrum of (a) an MR time series near the middle cerebral arteries and (b) a time series of a pulse oximeter placed on the subject's finger. The peaks in the power spectrum at 0.3 Hz (respiratory) and 1 Hz, 2 Hz, etc. (cardiac), are evident in both spectra. Biswal *et al.* (1996) demonstrated the presence of cardiac effects even at MR sampling rates much lower than the cardiac cycle.

In addition to fluctuations from cardiac and respiratory effects, the demonstrated dependence of BOLD-weighted MR signal on brain state (Kwong *et al.*, 1992; Ogawa *et al.*, 1992) implies that there should be fluctuations present in MR data due to uncontrolled fluctuations in brain state. Detailed studies of fMRI activation signal and stimulus timing show that a latency of several seconds is required to maximize oxygenation contrast (Menon *et al.*, 1994). This implies that only prolonged brain state changes generate a

large enough oxygenation signal to be easily observable with fMRI.

In 1995, Biswal *et al.* observed that the low frequency (<0.08 Hz) resting state fluctuations from single slice fMRI time series acquisitions are correlated between the left and right regions of motor cortex (Biswal *et al.*, 1995). This observation of spatiotemporal correlation constitutes a novel method for assessing functional connectivity in the human brain. Although "resting state," by default simply means "uncontrolled state," there is a potential advantage to a measure of functional connectivity which does not require a focal task. The hypothesis being tested is a very general one: Do two (or more) cortical regions have low-frequency fluctuations which have the same, or similar, phase in an awake subject? Biswal *et al.* observed that this hypothesis was supported for two cortical regions which are known to be anatomically connected. Since the rapid-sampled acquisitions they performed allow only a single slice to be studied, the generality of the hypothesis is limited by the anatomic region being sampled.

Biswal *et al.* performed their measurements using a local gradient coil. If these observations prove to be general, MRI may become a valuable tool for measuring functional connectivity, especially if extended from single-slice measurements to whole-brain studies. In addition, a measure of whole-brain connectivity in the resting state would allow researchers and clinicians to test a variety of connection hypotheses with data obtained from a single study.

In the present study, a 1.5-T whole-body EPI system was used to obtain single-slice and volumetric resting state data on three normal right-handed male subjects, in order to investigate the generalization of the measurement of these correlations to (1) less sensitive whole-body systems, (2) multislice acquisitions, and (3) other right/left symmetric cortical regions.

MATERIALS AND METHODS

All data were acquired with a standard birdcage RF coil and a 1.5-T GE Signa Horizon scanner (GE Medical Systems, Waukesha, WI) outfitted with fast gradients to allow whole-body echoplanar imaging. Subjects were recruited and scanned in a protocol described below. The protocol was designed to (1) confirm the observation of high correlation in resting state fluctuations between right and left hemisphere motor cortex in single slice, rapid TR acquisitions, (2) extend the observations to low sampling rate (TR = 2 s) multislice acquisitions, and (3) extend the observed correlations to other right/left symmetric functional cortices.

Subject Preparation

Three male subjects were recruited and scanned according to a protocol approved by the University of

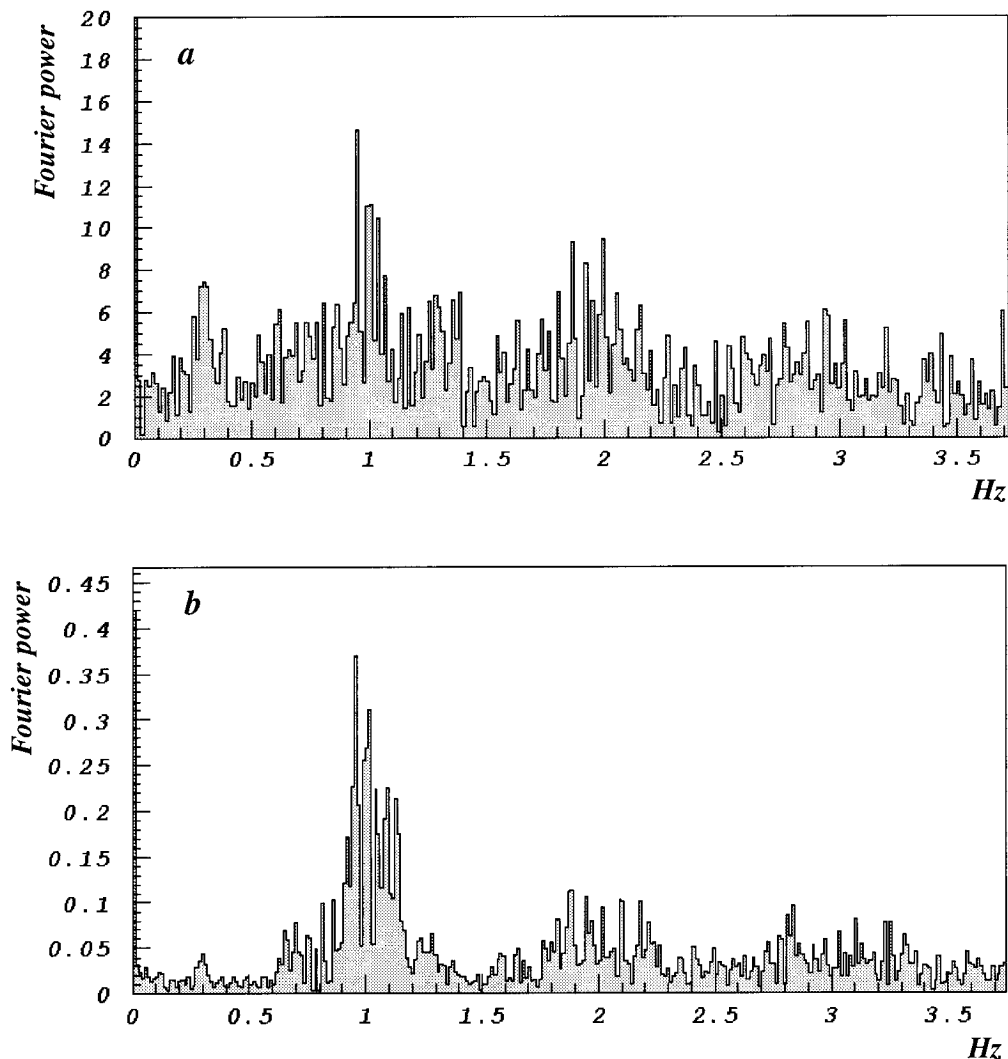


FIG. 1. Fourier power spectrum for (a) MR time series from a pixel near the middle cerebral arteries and (b) time series from a pulse oximeter. The respiratory peaks occur at 0.3 Hz and first harmonic cardiac peaks are at 1 Hz.

Wisconsin Internal Review Board (Protocol 94-832-193). The mean age was 33.8 years and no subjects were on medication of any kind at the time of the study. All subjects scored higher than +80 on the Edinburgh Inventory (Oldfield, 1971) and thus were considered to be strongly right-handed.

Two studies were performed on each subject—a single-slice rapid sampling rate study and a multislice low sampling rate study (described below).

Motion in Correlation Analyses

It is well known that gross head movement in BOLD-weighted fMRI acquisitions causes artifacts in a correlational analysis (Jiang *et al.*, 1995; Friston *et al.*, 1996a). Retrospective methods of realignment such as those proposed by Woods *et al.* (1993) and Friston *et al.* (1996a) will tend to increase spatiotemporal correla-

tions in data which contain only very low levels of motion and physiologic and systemic noise (see Fig. 2). Since our objective is to investigate the intrinsic spatio-temporal correlations present in BOLD-weighted fMRI time series, our approach toward accounting for possible motion effects was very conservative. A bite-bar was used to minimize head motion during the scanning sessions. A dental impression was taken immediately prior to scanning and a bar with the impression was affixed to the RF coil. All data were postprocessed for evidence of motion using the Automated Image Registration (AIR) package of Woods *et al.* (1993). Of all the studies performed, only one of the studies had a measured peak displacement of more than 0.4 mm. Peak motion was determined using the mean displacement over a parallelepiped contained within the imaged volume (Jiang *et al.*, 1995). The level of 0.4 mm was determined to be consistent with minimal gross head

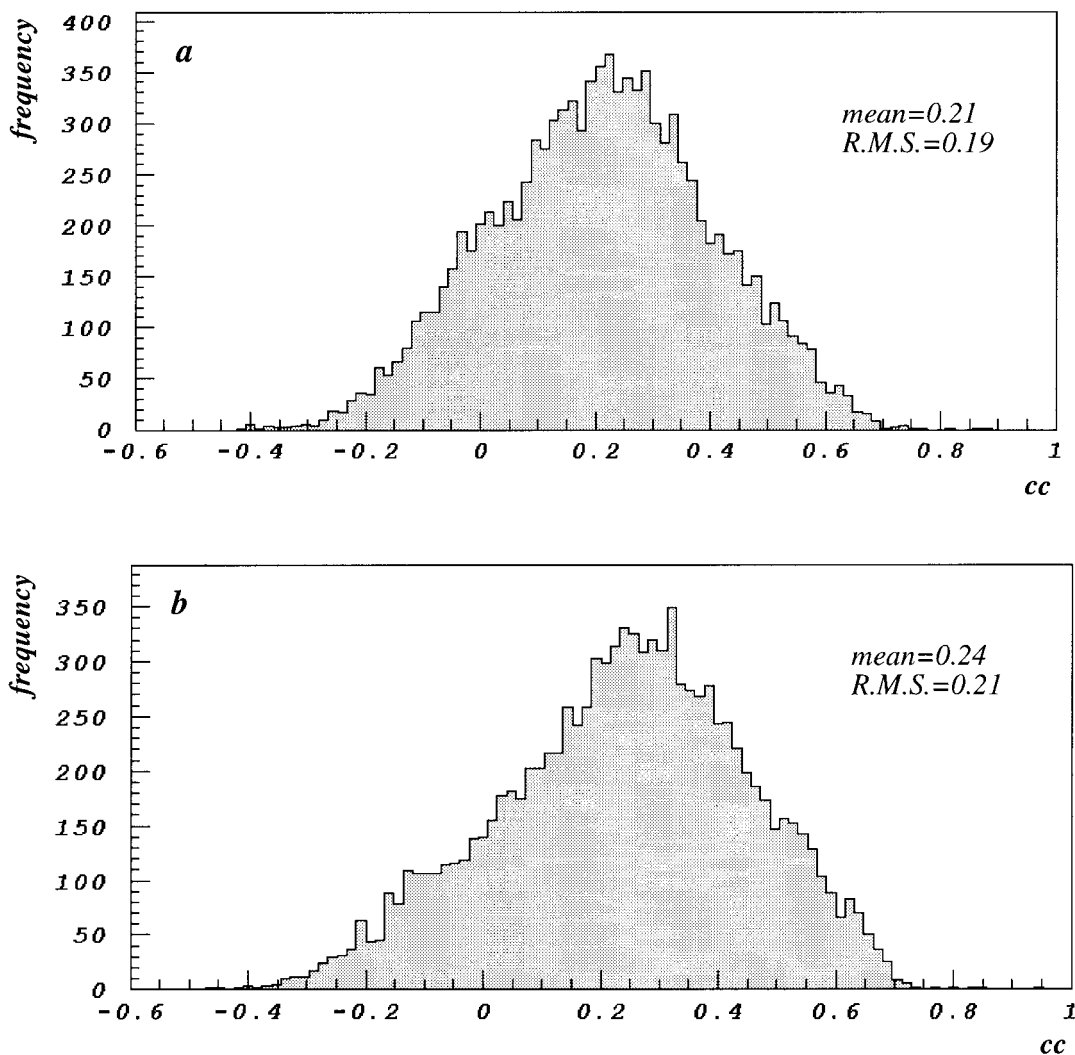


FIG. 2. Frequency distributions for the cross correlation of all pixels in a 15-slice, 512-repetition BOLD-weighted study, calculated according to Eq. (1). The same (x, y, z) pixel was used as the reference pixel in both (a) and (b). Graph (a) was calculated on data which were digitally filtered to remove frequencies above 0.08 Hz, but was not realigned to correct for motion effects. Graph (b) was also digitally filtered, but was realigned prior to filtering to correct for motion effects using the automated image registration algorithm of Woods *et al.* (1993). The data were acquired using a bite bar to restrict gross head motion as discussed in the text and no displacement was detected greater than 0.4 mm, measured according to the method of Jiang *et al.* (1995). The increase in the mean and RMS in the realigned data could be an indication of increased spatial and temporal correlations due to the alignment algorithm.

motion. The data set with detected motion above 0.4 mm was discarded and the remaining uncorrected data were assumed to be free from motion artifact. Based on this, the data shown here showed no evidence of gross head motion.

Imaging Protocol

In each scanning session, in addition to the functional scans which will be described below, the following high-resolution anatomical scans were performed.

Scan 1: 3D Spoiled GRASS Whole-Brain Scan

This scan was necessary to calculate Talairach landmarks (Talairach and Tournoux, 1988) in each subject's

data in order to permit intersubject combination of results. The scan parameters were matrix = 256×128 , field-of-view = 24×24 cm, echo time = 8 ms, repetition time = 35 ms, flip angle = 30° , slices = 124, slice thickness = 1.0 mm.

Scan 2: 3D Time-of-Flight Whole-Brain Vascular Scan

This scan was necessary to identify the location of large vessels in order to exclude regions where high-power cardiac and respiratory coupling to observed correlations may be expected. The scan parameters were: matrix = 512×192 , field-of-view = 24×18 cm, echo time = 2.3 ms, repetition time = 48 ms, flip angle = 30° , slices = 124, slice thickness = 1.0 mm.

Single-Slice Studies

Using the 3D spoiled GRASS anatomic scan, a single axial slice was prescribed through the precentral gyrus. The slice location was chosen in all cases to approximate the location of primary motor cortex associated with finger movement. The prescribed functional scan was gradient-echo echoplanar, matrix = 64×64 , field-of-view = 24×24 cm, echo time = 50 ms, repetition time = 134 ms, flip angle = 30° . In just over 5 min (5:08:12), 2300 images were acquired. The subjects were instructed to refrain from voluntary movement of any kind and to keep their eyes closed for the duration of the scan.

Previous reports of observed correlations in rapid TR, single slice resting-state studies utilized a total of 512 acquired images with a repetition time of 250 ms (Biswal *et al.*, 1995). After digital filtering frequencies above 0.08 Hz, the temporal degrees of freedom were dramatically reduced. In general, reducing the degrees of freedom will reduce the specificity of a correlation analysis, since the correlation coefficient distribution for the null hypothesis converges slowly to a Gaussian distribution with standard deviation $1/\sqrt{N}$, where N is the number of degrees of freedom (Press *et al.*, 1984). In order to improve suppression of background fluctuations, we acquired 2300 images.

Multislice Studies

Fifteen coronal slices, 7 mm thick with a 2-mm interslice gap were prescribed. The locations were chosen such that the brain was covered from the occipital pole to just anterior to the frontal horns of the lateral ventricles. The prescribed functional scan was gradient-echo echoplanar, matrix = 64×64 , field-of-view = 24×24 cm, echo time = 50 ms, repetition time = 2000 ms, flip angle = 90° . Five hundred thirty images were acquired at each location. Total scan time for each study was 17 min, 40 s. The subjects were instructed to refrain from voluntary movement of any kind and to keep their eyes closed for the duration of the scan.

Data Analysis

The raw spatial-frequency data from the functional studies was acquired and reconstructed offline. A Ham-

ming window was applied to the raw data. This increases the BOLD contrast-to-noise ratio with only a small loss of spatial resolution (Lowe and Sorenson, 1997).

Resting State Studies

Our hypothesis is that low-frequency fluctuations in the resting-state fMRI data are correlated between functionally related anatomical structures. In order to test this hypothesis we processed the data in three steps:

- (1) low-pass filtering,
- (2) selection of regions-of-interest,
- (3) correlation analysis.

Temporal Filtering

The resting state data from each pixel was passed through a finite-impulse response (FIR) filter to remove all frequencies above 0.08 Hz. This removes the oxygenation fluctuations from direct sampling of respiratory and cardiac-related oxygenation fluctuations.

Regions-of-Interest

The following locations, noted in millimeters, were chosen from the Talairach coordinates in each subject:

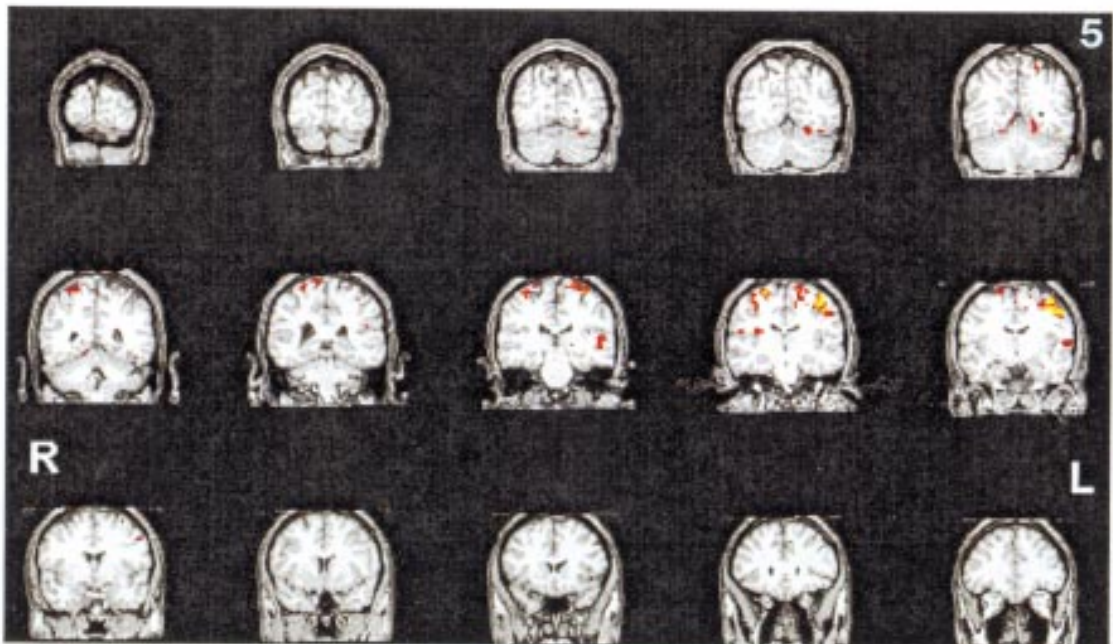
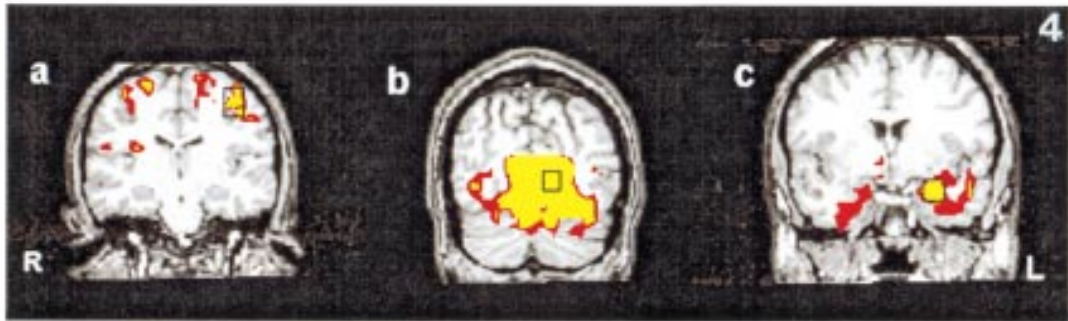
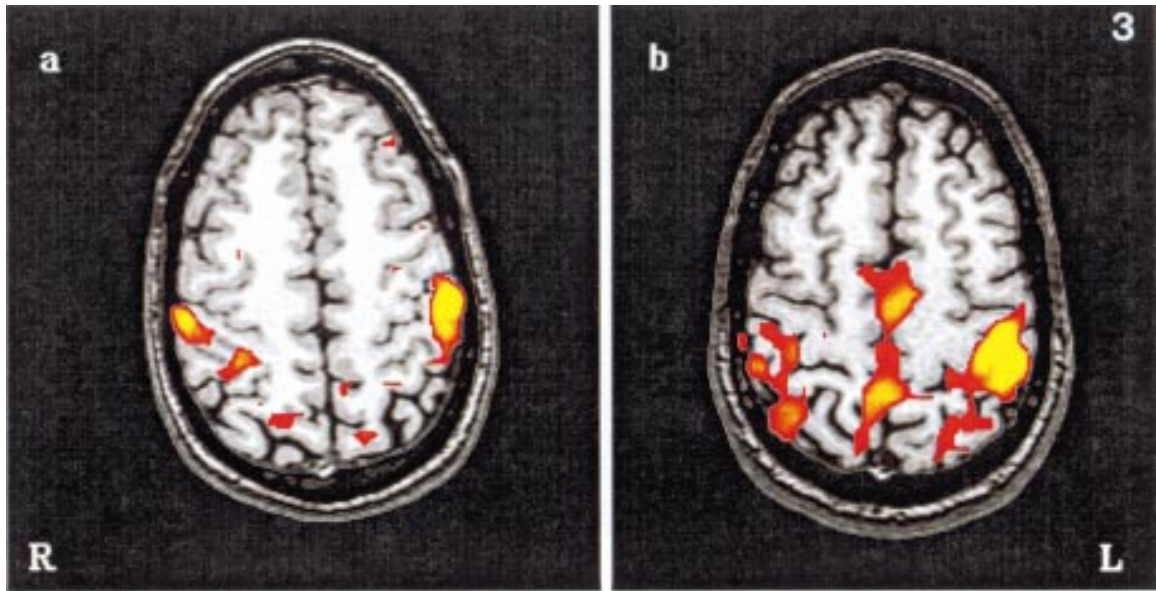
- (1) left precentral gyrus (Talairach coordinate $[-40, -12, 50]$),
- (2) left calcarine fissure (Talairach coordinate $[-10, -75, 10]$),
- (3) left amygdala (Talairach coordinate $[-20, -8, -10]$).

These regions were chosen to investigate the generality of the correlation method to different cortical and subcortical structures. The ROI was chosen carefully in each subject to avoid including pixels containing large vessels. This information was available from the vascular scan taken during each subject's scanning session. In each case, the ROI was 2 pixels square in-plane, and contained in one slice. The volume of tissue in each ROI was then $7.5 \times 7.5 \times 7$ mm. The reference time series was taken as the arithmetic average of the 4 pixels in the ROI.

FIG. 3. Maps of t_{corr} values rendered onto high resolution anatomical scans of the imaged region for two right-handed males. The t_{corr} values are calculated from the correlation coefficient to an ROI in the left precentral gyrus in each subject. The color scale is such that red corresponds to 10^{-5} and yellow corresponds to 10^{-20} . The right and left sides of the images are as indicated.

FIG. 4. Maps of χ^2 values for correlation with (a) left precentral gyrus, (b) left calcarine fissure, and (c), left amygdala from the multislice resting-state acquisition. Maps are combined for the three subjects as discussed in the text. The color scale is such that red corresponds to 10^{-5} and yellow corresponds to 10^{-20} . The right and left sides of the images are as indicated. The black box denotes the ROI which was chosen for the correlation calculation.

FIG. 5. Maps of χ^2 values for correlation with the left precentral gyrus from the three subjects rendered onto high resolution anatomical scans. The color scale is such that red corresponds to 10^{-5} and yellow corresponds to 10^{-20} . The right and left sides of the images are as indicated.



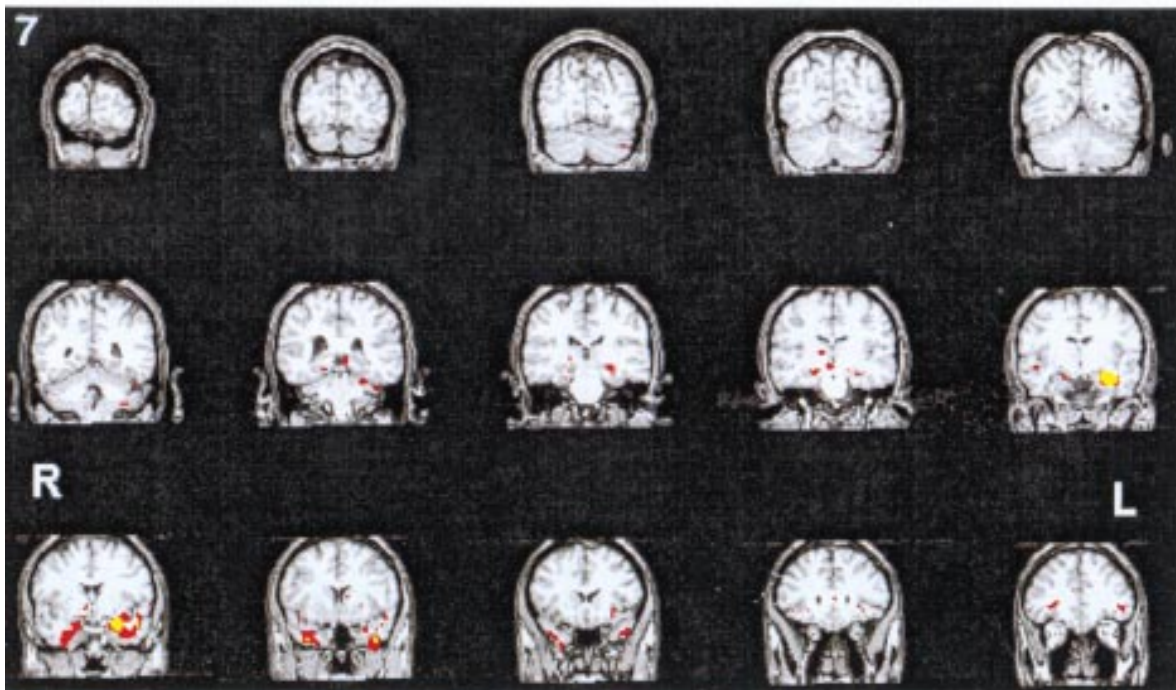
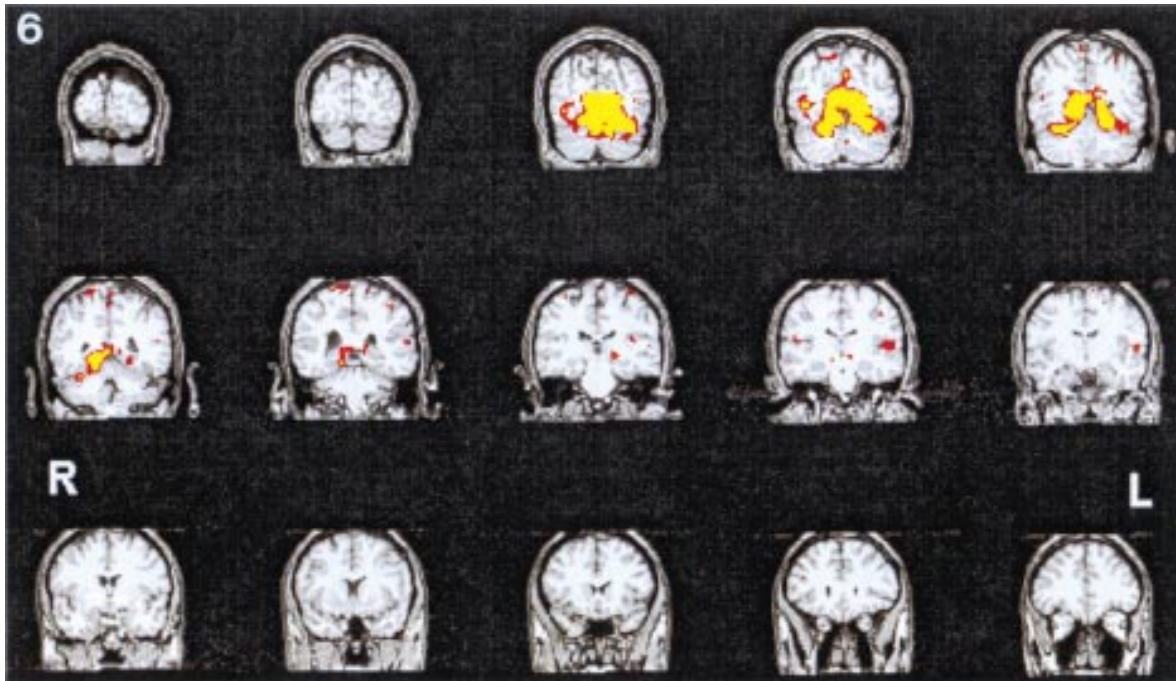


FIG. 6. Maps of χ^2 values for correlation with the left calcarine fissure from the three subjects rendered onto high resolution anatomical scans. The color scale is such that red corresponds to 10^{-5} and yellow corresponds to 10^{-20} . The right and left sides of the images are as indicated.

FIG. 7. Maps of χ^2 values for correlation with the left amygdala from the three subjects rendered onto high-resolution anatomical scans. The color scale is such that red corresponds to 10^{-5} and yellow corresponds to 10^{-20} . The right and left sides of the images are as indicated.

Correlation Analysis

The hypothesis which is the basis for analyzing the resting-state data is that the low-frequency temporal fluctuations in the data are correlated in regions which are functionally associated. To test this, we calculated the correlation coefficient for all pixels in the acquired volume, using the time series from a given region-of-interest as the reference time series,

$$cc = \frac{\sum_{i=1}^N (r(i) - \bar{R}) \cdot (S_i - \bar{S})}{\sqrt{\sum_{i=1}^N (r(i) - \bar{R})^2 \cdot \sum_{i=1}^N (S_i - \bar{S})^2}}, \quad (1)$$

where r is the reference time series and S is the signal for the given pixel. \bar{R} and \bar{S} are the average reference and current pixel signal levels, respectively. The summation was performed over all time points. *In vivo* fMRI time series data are known to have time and spatial correlations (Friston *et al.*, 1994). Thus, we expect that the distribution of the correlation coefficients will be skewed due to intrinsic time and spatial correlations from the imaging method. The distribution can differ depending on the ROI chosen as the reference in the correlation (this can be due to different spatial frequency characteristics as well as different couplings to cardiac, respiratory, or other physiologic “noise”). In order to normalize the distributions, a correction procedure was performed which is outlined in Appendix 1. The result is a Z -statistic.

Combination of Multislice Results

The multislice maps are combined across the three subjects to produce a map of χ^2 in a manner outlined in Appendix 2. Thresholds were chosen such that a single-pixel significance of 10^{-5} was required. This threshold was chosen based on the fact that approximately 2×10^5 brain tissue pixels were cross-correlated in each study. Although our *a priori* region of interest, i.e., the homologous region of cortex to the reference region, consists of only a few pixels, this threshold ensures that very few pixels will pass due to random background fluctuations.

RESULTS AND DISCUSSION

Figure 3 shows the results of the single-slice studies for two of the three subjects. In both cases, the homologous region of the precentral gyrus is among the highest correlated pixels in the slice. The third subject's results are not shown because those data had detected

motion levels above 0.4 mm.³ The threshold for each map was chosen such that a significance of 10^{-5} was required. This threshold was chosen to be consistent with the threshold chosen for the multislice study. The color scale is such that red corresponds to significance level of 10^{-5} and yellow corresponds to 10^{-20} .

Figure 4 shows the results of the χ^2 analysis on the multislice data combined across the three subjects. Shown are the χ^2 maps for each of the ROIs for the slice containing the ROI. The threshold for each map was chosen such that a significance greater than 10^{-5} was required. The maps are rendered in the same false color scale onto high-resolution anatomic images. The color scale is the same in all three figures: red corresponds to 10^{-5} and yellow corresponds to 10^{-20} . Figure 4a shows that the homologous region in the precentral gyrus is still among the most highly correlated regions in the lower sampling rate, multislice acquisition. Figures 4b and 4c show that the right/left correlations which are observed between the two hemispheres' motor cortices are also present between right and left calcarine fissure (visual cortex) and right and left hemisphere amygdalae.

Figures 5, 6, and 7 show the whole-head χ^2 maps from the multislice studies rendered onto high-resolution anatomic images from a single subject. The threshold and color scales are as in Fig. 4.

The MR acquisition method used for the multislice data acquired each slice in the volume at evenly spaced intervals throughout the repetition time of 2 s. This means that there was a 2-s delay between the acquisition of the first acquired slice in the volume and the last acquired slice. In the unfiltered data, this could introduce a bias in the correlation coefficient between correlated signals across slices. Simulations were run to verify that after filtering frequencies above 0.08 Hz, the correlation coefficient is insensitive to temporal offsets up to 2 s for a signal with a frequency spectrum equivalent to that measured *in vivo*.

Inspection of Figs. 5, 6, and 7 shows that, in addition to the homologous region of cortex, there are a number of intra- and interhemispheric regions which appear to be highly correlated and which belong to anatomic structures which are known from paradigm-based functional neuroimaging studies (i.e., studies involving execution of a task) and deep-implantation EEG studies on animals to have functional involvement in similar tasks. In particular, the left precentral gyrus (Fig. 5) has high correlation to the postcentral gyrus and a small region of the left-hemisphere thalamus, which were shown to be involved in a motor task by Strother *et al.* (1995). The calcarine fissure (Fig. 6) has high correlation to the extended occipital cortex (McIntosh *et*

³ This subject's multislice study did not show evidence of gross head motion and was included in the multislice study analysis.

al., 1994). The amygdala (Fig. 7) has high correlation to the hippocampus and the inferior temporal lobe as well as a small region of the right hemisphere thalamus (Pare *et al.*, 1995).

In summary, Figs. 4–7 show that the high correlation of low-frequency fluctuations between right and left hemisphere-symmetric cortical regions is not only generalized to visual cortex and amygdala, but is present in lower sampling rate, whole-head acquisitions. The specificity of the correlations appears to be somewhat reduced compared to those observed in the single-slice study. This *a posteriori* observation was more precisely tested in the following way: a single coronal slice was prescribed which passed through the left and right precentral gyri and the right inferior parietal lobe (rIPI) of a single subject. The right precentral gyrus (rPreC) is simple motor cortex, while rIPI is not expected to be involved in simple motor function. Four acquisitions were prescribed at different sampling rates and the correlation coefficient to the left precentral gyrus is calculated in each case for rPreC and rIPI. The number of images acquired in each scan was set such that approximately the same number of sampled frequencies remained after filtering frequencies above 0.08 Hz. This was done to try to minimize the effect of changing the effective degrees of freedom remaining after filtering, since, as stated above, the specificity of the correlation coefficient depends on the degrees of freedom. Table 1 shows the results. Column 5 of Table 1 shows that, although the magnitude of the correlation of the homologous region stays approximately the same, putative background correlations become higher with increasing TR.⁴ This is most likely due to the lack of specificity in the 0.08-Hz FIR filter for the longer sampling times. Once the cardiac and respiratory rates are no longer directly sampled, these effects can alias into frequencies below 0.08 Hz. In this case, the FIR filter will not remove these effects and the correlational analysis will be affected.

As an example of this, we consider a respiratory rate of 0.28 Hz. This corresponds to 16 breaths per minute, which is a normal breathing pattern. Any effect which is modulated at this rate, but sampled at 0.5 Hz (as in a TR = 2 s BOLD-weighted fMRI study), will see a fundamental frequency aliased to 0.06 Hz. This will pass our 0.08-Hz filter and increase the correlation of pixels with a similar respiratory-cycle sensitivity. Cardiac-

⁴ It should be pointed out that although Table 1 is in apparent disagreement with Fig. 5, i.e., that the correlation of low-frequency fluctuations between homologous regions of precentral gyrus cannot be detected at TRs of 2 s, Fig. 5 is the result of combining the correlation analysis across three subjects, whereas Table 1 is generated from a single subject. The combination across subjects increases the statistical power such that the underlying correlations can be discriminated.

TABLE 1

Correlation Coefficient Between Left Precentral Gyrus and Right Precentral Gyrus cc_{rPreC} and Left Precentral Gyrus and Right Inferior Parietal Lobe cc_{rIPI}

TR (ms)	Frequencies		cc_{rPreC}	cc_{rIPI}	Ratio
	passing 0.08-Hz filter				
133.4	44		0.73	0.24	3.0
600	51		0.87	0.53	1.6
2000	43		0.73	0.69	1.1
4000	43		0.86	0.57	1.5

Note. The last column is the ratio of columns 3 and 4. See the text for discussion.

cycle effects can alias into the low-sampling rate acquisitions as well. Figure 8b shows the frequency spectrum from a pulse oximeter probe placed on a subject's fingertip. The pulse oximeter was sampled at 100 Hz. Figure 8b was constructed by resampling the observed waveform at 0.5 Hz—corresponding to the sampling rate for an MR acquisition with TR = 2 s. The structure in the center of the spectrum is clearly from aliased cardiac and respiratory effects. Although it is difficult to distinguish from instrument noise, there is some structure below 0.08 Hz which could be due to cardiac and/or respiratory effects and which would pass our 0.08-Hz filter.

As stated in Appendix 1, the effective degrees of freedom in time series data acquired at a given sampling rate depends on the underlying spectral density of the imaged tissue. In this study, we acquired two data sets on each subject, one sampled at ~7.5 Hz and one sampled at 0.5 Hz. Thus, we sampled the spectral density with 2300 points from 0 to 3.75 Hz (resolution = 0.0016 Hz) and 530 points from 0 to 0.25 Hz (resolution = 0.00047 Hz). We then examined the spatiotemporal correlations after discarding frequencies higher than 0.08 Hz in both studies. Our spectral resolution for the spectral density function is almost four times greater in the lower sampling rate data. Although fewer data points are acquired, except for the aliasing effects from undersampling high-frequency physiologic effects, characterization of the spectral region of interest is greater in the low sampling rate volumetric acquisitions.

It should be mentioned that these aliased effects will, in general, depend on the exact nature of the subject's respiration and cardiac cycles. This implies that they cannot be considered to be stable in time or across changes in brain state. It is well known that some behavioral paradigms affect cardiac and respiratory rates in subjects (Lang *et al.*, 1993; Shea, 1996) and in these cases the aliased effects which are increasing the background correlations will change. Parallel measurement of these physiologic noise sources at a sampling rate higher than their Nyquist frequency is a possible

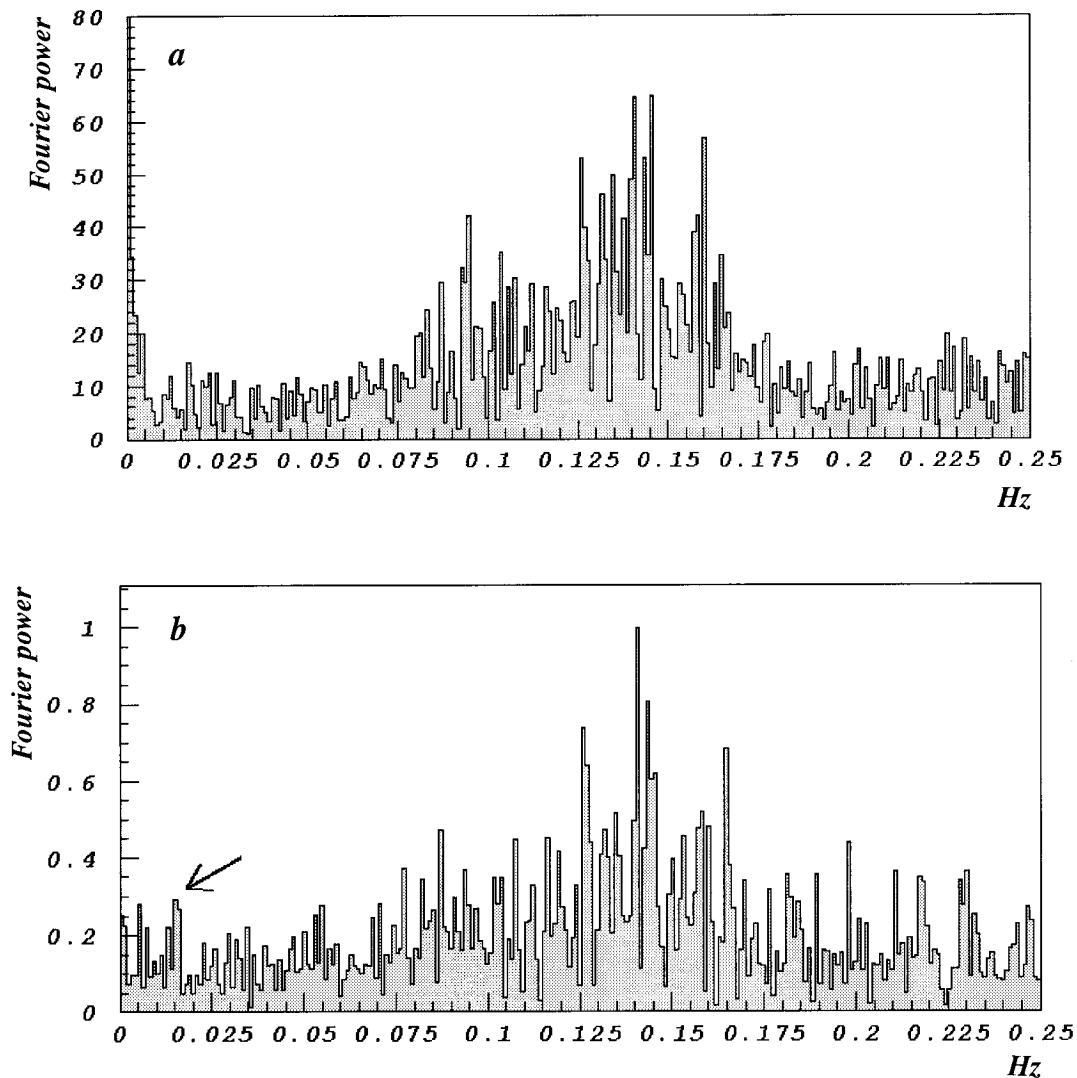


FIG. 8. Fourier power spectrum for (a) MR time series from a pixel near the middle cerebral arteries and (b) time series from a pulse oximeter. The sampling rate for both spectra was 0.5 Hz. The structure in the center of both spectra is from aliased cardiac and respiratory oxygenation fluctuations. The arrow indicates a possible aliased effect which would pass the 0.08-Hz low-pass filter.

method for retrospectively filtering these background effects. However, the slight variations in respiratory and cardiac rate, as well as the asymmetric shape and narrow duty cycle of the cardiac rate-induced oxygenation pulse make it difficult to calculate the aliasing effects precisely. The present study required the combination of three subjects' data to reveal the spatiotemporal correlation between right and left hemisphere symmetric cortices. Successful removal of the aliasing effects from undersampled cardiac and respiratory oxygenation fluctuations should allow single-subject determination of functional connectivity in whole-brain studies.

CONCLUSION

We have confirmed a previous report of high correlations in low-frequency fluctuations in the resting state

between right and left hemisphere motor cortices in high sampling rate, single-slice echoplanar acquisitions. In addition, we have shown that these high correlations are preserved in lower sampling rate, multislice echoplanar data. In single volumetric scanning sessions in three human subjects, high correlations were observed between right and left hemisphere precentral gyri (motor cortex), right and left hemisphere calcarine fissures (visual cortex), and right and left hemisphere amygdalae. These observations indicate that the phenomenon of low-frequency correlations in resting-state data is most likely a general property of right/left symmetric functional cortices. Our extension of this observed effect to multislice acquisitions allows for the possible assessment of whole-brain functional connectivity.

The loss of specificity in these correlations in the

multislice acquisitions from those observed at higher sampling rates appears to be due to aliased respiratory and cardiac effects which are not completely suppressed by the 0.08-Hz cutoff low-pass filter.

APPENDIX 1: CORRECTION OF CORRELATION COEFFICIENT

The correlation coefficient distribution for the null hypothesis converges slowly to a Gaussian distribution with standard deviation $1/\sqrt{N}$, where N is the number of degrees of freedom (Press *et al.*, 1984). This is undesirable behavior as a general test statistic being used across many studies which potentially have different degrees of freedom (e.g., different numbers of images, TRs, etc.). There is an algebraic relationship between a t statistic and the correlation coefficient which is approximately true for distributions with more than 20 degrees-of-freedom (see Eq. (A1)). The t statistic converges to a standard Normal distribution (i.e., mean = 0 and standard deviation = 1) for degrees-of-freedom greater than ~ 20 . Thus, confidence levels for a given t value remain relatively stable across many experimental conditions, making it a desirable test statistic.

The presence of physiologic-based fluctuations (e.g., cardiac and respiratory induced) as well as spatial correlations in fMRI data causes distortions in the cross-correlation coefficient distribution to other brain pixels for any given pixel in resting-state acquisitions. A source of these distortions is that the effective temporal degrees of freedom will vary spatially. The effective degrees of freedom for data sampled at a given rate depends on the spectral density of the sampled tissue (Friston *et al.*, 1994). The fact that the spectral distribution of BOLD-weighted time series data is generally not white and varies spatially has been reported by several groups (Weisskoff, 1993; Biswal *et al.*, 1996). In *in vivo* data, the spectral density will not be the same across individuals, across trials in the same subject (due to the variability of cardiac, respiratory-cycles, etc.), or across pixels within the same study.

We adopt an empirical approach in dealing with the distortions to the correlation coefficient distribution. In order to allow us to use the same confidence-level threshold across subjects, it is necessary to normalize the effects of the intrinsic correlations. Also, as stated above, a Student's t statistic is desirable because the null hypothesis distribution is easily characterized as standard normal. We derive a normally distributed Student's t parameter, which can be thought of as a Z -statistic, from the cross-correlation calculation (Eq. (1)) in the following way:

(1) The correlation coefficient was transformed to a

Student's t according to:

$$t = \frac{cc}{\sqrt{cc^2 + v^2}}, \quad (\text{A1})$$

where cc is the correlation coefficient defined in Eq. (1) and v is the number of degrees of freedom—which we take to be the number of acquired time points. This was done to transform to a distribution which, for large v , should be standard normal (Eadie *et al.*, 1971). It should be noted that the distribution will not, in general, be normal at this point due to intrinsic effects discussed above.

(2) In order to correct the resulting t distribution, a three-parameter least-squares fit of the t distribution from each ROI was made to a Gaussian function. The free parameters were the mean, standard deviation, and area. The fit was restricted to the full-width at half-maximum (FWHM) of the t distribution. The assumption was that the t distribution consists of a Gaussian-distributed component from bulk system and physiologic correlations, plus a tail from higher-order correlations. The fit was restricted to the FWHM in order to attempt to fit only the Gaussian component. In all cases, the fit was required to have a χ^2 probability greater than 0.05.

(3) A corrected t , or a Z -statistic was calculated from the mean ($\langle t \rangle$) and standard deviation (σ) from the Gaussian fit:

$$z = t_{\text{corr}} = \frac{t - \langle t \rangle}{\sigma}. \quad (\text{A2})$$

Figure 9 shows the t and t_{corr} distributions for a single slice, 2300 repetition resting-state scan. The reference was an ROI in the left precentral gyrus of the slice. The t_{corr} distribution has been well corrected to a standard normal distribution by the above procedure.

APPENDIX 2: COMBINATION OF MULTISLICE DATA

The multislice maps are combined across the three subjects in the following way: The maps are calculated for the three ROIs for all three subjects. Each map is then transformed into Talairach coordinates using high-resolution three-dimensional whole-head data taken at the beginning of the scanning session. A combined map for each ROI is then formed by summing the square of the t_{corr} values for each subject, pixel-by-pixel. An important consequence arises from combining the data in this way. Summing the square of the t values ignores the importance of the *sign* of the correlation; that is, negative correlations and positive correlations are considered equally. Although high negative correlations are potentially very interesting (Nyberg *et al.*, 1996),

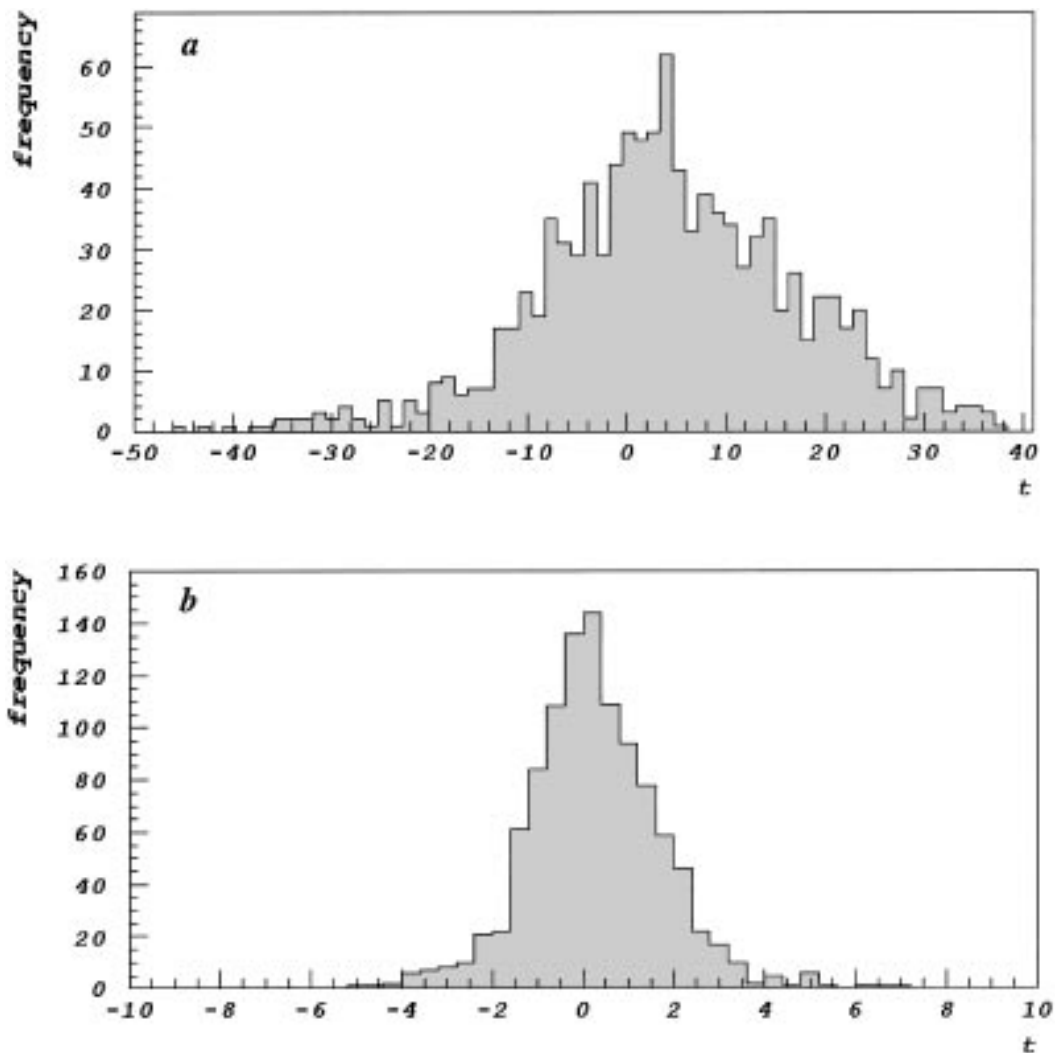


FIG. 9. Student's t distribution for all pixels to a timeseries of a pixel in the precentral gyrus of a single subject. t -values are calculated from the correlation coefficient according to Eq. 1. (a) is the distribution of t values before correcting to a Gaussian and (b) is the distribution after correcting.

they are certainly of a different nature than positive correlations.

In order to constrain our study to positive correlations, a positivity condition was applied to each map to assure that only positive correlations (i.e., $t_{\text{corr}} > 0$) were combined. If no positivity constraint had been applied, the final map for each ROI which would be a statistical parameter distributed approximately as a χ^2 with 3 *degrees-of-freedom* for the null hypothesis (i.e., correlations due to chance fluctuations). The positivity constraint distorted the statistics, so the significance levels were calculated using a Monte-Carlo simulation.

Monte Carlo Simulation

We wished to determine the single-pixel cumulative distribution function (CDF) for combining single-pixel t

values according to

$$\chi'^2(x, y, z) = \begin{cases} \sum_{i=1}^3 t_i^2(x, y, z) & t_i > 0 \text{ for all } i \\ 0 & t_i < 0 \text{ for any } i, \end{cases}$$

where $t_i(x, y, z)$ is the corrected t value for the Talairach-transformed data at pixel (x, y, z) in each of three *independent* studies. For our temporal degrees-of-freedom, we assumed that the t distribution for the null hypothesis was normal at each point and generated random deviates from a standard normal distribution in triples (Press *et al.*, 1984).⁵ If all t values in the triple

⁵ Please note that the procedure described in Appendix 1 ensures that the distribution of t values is Normal.

exceeded 0.05, we bin the sum of the squares. One million triples were generated. The resulting CDF showed that $\chi^2 > 20$ corresponded to a significance $< 10^{-5}$.

ACKNOWLEDGMENTS

The authors thank Richard J. Davidson and Patrick A. Turski of the University of Wisconsin for their advice in performing this study. Thanks are also given to Gary D. Hutchins and Vincent P. Mathews of Indiana University for their helpful comments on the manuscript.

This work was supported in part by NRSA Grant T32 CA09206, University of Wisconsin Radiological Sciences Training Grant.

REFERENCES

- Biswal, B., Yetkin, F. Z., Haughton, V. M., and Hyde, J. S. 1995. Functional connectivity in the motor cortex of resting human brain using echo-planar MRI. *Magn. Res. Med.* **34**:537–541.
- Biswal, B., DeYoe, E. A., and Hyde, J. S. 1996. Reduction of physiological fluctuations in fMRI using digital filters. *Magn. Res. Med.* **35**:107–113.
- Davidson, R. J., Leslie, S. C., and Saron, C. 1990. Reaction time measures of interhemispheric transfer time in reading disabled and normal children. *Neuropsychologia* **28**:471–485.
- Davidson, R. J., and Saron, C. 1992. Evoked potential measures of interhemispheric transfer times in reading disabled and normal boys. *Dev. Neuropsychol.* **8**:261–277.
- Eadie, W. T., Dryard, D., James, F. E., Roos, M., and Sadoulet, B. 1971. *Statistical Methods in Experimental Physics*. North-Holland, Amsterdam.
- Farber, D. A., and Knyazeva, M. G. 1991. Electrophysiological correlates of interhemispheric interaction in ontogenesis. In *Pediatric Behavioral Neurology* (G. Ramaekers and C. Njiokiktjien, Eds.), pp. 86–99. Suyi, Amsterdam.
- Friston, K. J., Frith, C. D., Liddle, P. F., and Frackowiak, R. S. J. 1993. Functional connectivity: The principal component analysis of large (PET) data sets. *J. Cereb. Blood Flow Metab.* **13**:5–14.
- Friston, K. J., Jezzard, P., and Turner, R. 1994. Analysis of functional MRI time-series. *Hum. Brain Mapping* **1**:153–171.
- Friston, K. J., Howard, W. S., Frackowiak, R. S., and Turner, R. 1996a. Movement-related effects in fMRI time-series. *Magn. Res. Med.* **35**(3):346–355.
- Friston, K. J., Frith, C. D., Fletcher, P., and Liddle, P. F. 1996b. Functional topography: Multidimensional scaling and functional connectivity in the brain. *Cereb. Cortex* **6**:156–164.
- Horwitz, B. 1991. Functional interactions in the brain: Use of correlation between regional metabolic rates. *J. Cereb. Blood Flow Metab.* **11**:A114–A120.
- Jezzard, P., LeBihan, D., Cuenod, D., Pannier, L., Prinster, A., and Turner, R. 1992. An investigation of the contribution of physiologic noise in human functional MRI studies at 1.5 tesla and 4 tesla. In *Proceedings, Society of Magnetic Resonance in Medicine 12th Annual Meeting, New York*, p. 1392.
- Jiang, A., Kennedy, D. N., Baker, J. R., Weisskoff, R. M., Tootell, R. B. H., Woods, R. P., Benson, R. R., Kwong, K. K., Brady, T. J., Rosen, B. R., and Belliveau, J. W. 1995. Motion detection and correction in functional MR imaging. *Hum. Brain Mapping* **3**:224–235.
- Koeda, T., Knyazeva, M., Njiokiktjien, C., Jonkman, E. J., De Sonneville, L., and Vildavsky, V. 1995. The EEG in acallosal children. Coherence values in the resting state: Left hemisphere compensatory mechanism? *Electroencephalogr. Clin. Neurophysiol.* **95**:397–407.
- Kwong, K. K., Belliveau, J. W., Chesler, D. A., Goldberg, I. E., Weisskoff, R. M., Poncelet, B. P., Kennedy, D. N., Hoppel, B. E., Cohen, M. S., Turner, R., Cheng, H. M., Brady, T. J., and Rosen, B. R. 1992. Dynamic magnetic resonance imaging of human brain activity during primary sensory stimulation. *Proc. Natl. Acad. Sci. USA* **89**:5675–5679.
- Lang, P. J., Greenwald, M. K., Bradley, M. M., and Hamm, A. C. 1993. Looking at pictures: Affective, facial, visceral, and behavioral reactions. *Psychophysiology* **30**(3):261–273.
- Lowe, M. J., and Sorenson, J. A. 1997. Spatially filtering functional magnetic resonance imaging data. *Magn. Res. Med.* **37**:723–729.
- McIntosh, A. R., Grady, C. L., Ungerleider, L. G., Haxby, J. V., Rapoport, S. I., and Horwitz, B. 1994. Network Analysis of cortical visual pathways mapped with PET. *J. Neurosci.* **14**(2):655–666.
- Menon, R., Hu, X., Mitra, P., Ogawa, S., and Ugurbil, K. 1994. Signal characteristics in function MRI of the brain upon visual stimulation. *Soc. Neurosci. Abst.* **20**:148.
- Nielson, J., Montplaisir, J., and Lassonde, M. 1993. Decreased interhemispheric EEG coherence during sleep in agenesis of the corpus callosum. *Eur. Neurol.* **33**:173–176.
- Nyberg, L., McIntosh, A. R., Cabeza, R., Nilsson, L.-G., Houle, S., Habib, R., and Tulving, E. 1996. Network analysis of positron emission tomography regional cerebral blood flow data: Ensemble inhibition during episodic memory retrieval. *J. Neurosci.* **16**(11):3753–3759.
- Ogawa, S., Tank, D. W., Menon, R., Ellerman, J. M., Kim, S. G., Merkle, H., and Ugurbil, K. 1992. Intrinsic signal changes accompanying sensory stimulation: Functional brain mapping with magnetic resonance imaging. *Proc. Natl. Acad. Sci. USA* **89**:5951–5955.
- Oldfield, R. C. 1971. The assessment and analysis of handedness: The Edinburgh inventory. *Neuropsychologia* **9**:97–114.
- Pare, D., Dong, J., and Gadreau, H. 1995. Amygdalo-entorhinal relations and their reflection in the hippocampal formation: Generation of sharp sleep potentials. *J. Neurosci.* **15**:2482–2503.
- Paus, T., Jech, R., Thompson, C. J., Comeau, R., Peters, T., and Evans, A. C. 1997. Transcranial magnetic stimulation during positron emission tomography: A new method for studying connectivity of the human cerebral cortex. *J. Neurosci.* **17**(9):3178–3184.
- Press, W. H., Teukolsky, S. A., Vetterling, W. T., and Flannery, B. P. 1984. *Numerical Recipes: The Art of Scientific Computing*. Cambridge Univ. Press, Cambridge.
- Scher, M. S., Sun, M., Steppe, D. A., Guthrie, R. D., and Scwabassi, R. J. 1994. Comparisons of EEG spectral and correlation measures between healthy term and preterm infants. *Pediatr. Neurol.* **10**(2):104–108.
- Shea, S. A. 1996. Behavioral and arousal-related influences on breathing in humans. *Exp. Physiol.* **81**(1):1–26.
- Sidtis, J. J., Volpe, B. T., Holtzmann, J. D., Wilson, D. H., and Gazzaniga, M. S. 1981. Cognitive interaction after staged callosal section: Evidence for transfer of semantic activation. *Science* **212**:344–346.
- Strother, S. C., Anderson, J. R., Schaper, K. A., Sidtis, J. J., Liow, J.-S., Woods, R. P., and Rottenberg, D. A. 1995. Principal component analysis and the scaled subprofile model compared to intersubject averaging and statistical parametric mapping. I. “Functional Connectivity” of the human motor system studied with [¹⁵O]Water PET. *J. Cereb. Blood Flow Metab.* **15**:738–753.
- Talairach, J., and Tournoux, P. 1988. *Co-Planar Stereotaxic Atlas of the Human Brain*. Thieme Medical, New York.
- Thatcher, R. W., Krause, P. J., and Hrybyk, M. 1986. Cortico-cortical associations and EEG coherence: A two-compartmental model. *Electroencephalogr. Clin. Neurophysiol.* **64**:123–143.

- Tucker, D. M., Roth, D. L., and Bair, T. B. 1986. Functional connections among cortical regions: Topography of EEG coherence. *Electroencephalogr. Clin. Neurophysiol.* **63**:242–250.
- Weisskoff, R. M., Baker, J., Belliveau, J., Davis, T. L., Kwong, K. K., Cohen, M. S., and Rosen, B. R. 1993. Power spectrum analysis of functionally-weighted MR data: What's in the noise? In *Proceedings Society of Magnetic Resonance in Medicine 12th Annual Meeting, New York*, p. 7.
- Woods, R. P., Mazziotta, J. C., and Cherry, S. R. 1993. MRI-PET registration with automated algorithm. *J. Comput. Assist. Tomogr.* **17**:536–546.